Contribution to the understanding of the performance differences between commercial current collectors in Li–S batteries

A. Benítez[a], F. Luna-Lama[a], A. Caballero[a], E. Rodríguez-Castellón[b], J. Morales[a*]

[a] Dpto. Química Inorgánica e Ingeniería Química, Instituto Universitario de Nanoquímica (IUNAN), Universidad de Córdoba, 14071 Córdoba, Spain

[b] Dpto. de Química Inorgánica, Cristalografía y Mineralogía, Facultad de Ciencias, Universidad de Málaga, 29071 Málaga, Spain

*Corresponding author. E-mail address: iq1mopaj@uco.es (J.M)

Abstract

Lithium–sulfur batteries have been recognised as highly promising next-generation batteries, due to their low cost and high theoretical energy density. Despite numerous advances in this technology over the last decade, its commercialisation is still a challenge that has not yet been achieved. Many efforts have been made to improve the problems that these batteries present, mainly by investigating different cathode manufacturing strategies, testing novel Li anodes, new additives in the electrolytes, and modified separators or interlayers. However, the characteristics of the current collectors used in the preparation of the electrodes have been rarely addressed. Three commercial collectors are commonly used in basic research on Li–S batteries: Al foil, carbon coated Al foil (Al-C), and carbon paper (gas diffusion layer, GDL). In this work, a detailed study of the electrochemical response of these commercial collectors has been carried out. The tests were carried out on two S composites formed by carbons of a different natures, commercial carbon black and synthetic N-doped graphene. In addition, the S impregnation method was different, using either melt diffusion at 155 ºC or ethylenediamine as S solvent, respectively. In both systems, the results were similar – the electrodes

supported on GDL delivered higher specific capacities than those supported on Al and Al-C, with minimal differences between the two. Of the different collector properties examined to explain this behaviour, namely Al corrosion, electrical conductivities, surface-level composition, and surface texture, only the latter had a significant effect in the performance of GDL-based electrodes. SEM images revealed a rough and cracked surface formed by the agglomerated carbon particles that give rise to a complex pore system, predominantly consisting of macropores. All of these features are beneficial for a better anchoring of the active material on the collector surface, in addition to enhancing the wettability of the electrolyte and favouring reaction kinetics. In contrast, the Al-based collector possesses a very smooth and non-porous surface, detrimental to both the active material-substrate interface and the active material impregnation by the electrolyte.

Keywords: Current collector; Carbon paper; Aluminum foil; Lithium–sulfur battery

1. Introduction

Since its commercialisation at the end of the last century, the Li-ion battery (LIB) has imposed its unquestionable hegemony in the information and communications technology sector, compared to other types of non-Li-based rechargeable batteries. Difficulties arise in its adoption in the transport sector, as it is unlikely that the Li-ion battery exceeds 600 Wh kg^{-1}, an energy value too low for vehicles to have an acceptable range of autonomy [1,2]. As is well-known, LIBs use graphite as the anode and Li ions inserted in an inorganic matrix which acts as the cathode, with Li ions capable of being reversibly extracted. However, the advantages of Li in electrochemical storage energy systems are unquestionable, due to its low potential (-3.03 V), high specific gravimetric (3861 mAh g^{-1}), and

volumetric (2062 mAh cm^{-3}) capacity [3]; hence, great attention continues to be paid to other reversible reactions of the element. One example is the reaction between Li and S to give Li_2S, whose specific capacity and energy are 1675 mA h g^{-1} and 2600 Wh kg^{-1}, respectively, much higher than that of LIBs (e.g., 387 W h kg^{-1} for typical $LiCoO_2$/graphite pair [4]). Other advantages of S are its abundance, low cost and environmental friendliness [5]. All of these advantages are offset by several drawbacks, with the three main drawbacks being: (i) the insulating properties of S and of the final reaction products (Li_2S/Li_2S_2); (ii) the solubility of the intermediate polysulphides in the electrolyte (shuttle effect), and (iii) the volumetric expansion (~80%) from S to Li_2S. These hindrances lead to a low rate performance, low utilisation of S, and degradation of cycle life, among other effects detrimental to high-quality battery operations. To overcome these obstacles, several proposals have been reported in recent years, which has also resulted in numerous reviews describing the state-of-the-art of this type of battery [6–17]. In these reviews, focus is paid not only to exhaustive treatments of the different systems added to S to improve the system conductivity, trap polysulphides, and act as buffers for volume changes (carbons, polymers, inorganic-based compounds such as oxides, hydroxides, metal organic framework, nitrides, among others), but also to treatments of the electrolyte and the battery anode.

A component that has been paid less attention is the current collector, which plays an indisputably relevant role in battery operation. To our knowledge, there are few reviews focussed on these battery components, and they are more oriented to free-standing 3D systems based on nanostructured carbons in the form of nanotubes, nanofibers, graphene, etc [18–20]. In this context, Manthiram's group has been especially active testing different current collectors based on porous carbons of different origin and using high sulfur loading (around 2 mg cm^{-2}) [21–23]. Especially scarce are comparative studies on the behaviours of different current collectors used in the deposition of cathodic material for Li–S batteries. Only in ref. [11] does a short section on flexible electrodes oriented to make freestanding S cathodes, a prerequisite to a flexible battery, appear. In general, they are prepared from 1D carbons, to favour both the transport of electrons and the formation of an interconnected framework [24–26],

and can confine a high S loading, preferably impregnated with catholytes as sources of S. Based on our information, Chung and Manthiram [22] were the first to find a severe capacity fade of an Al foil current collector, compared with a porous carbon current collector, although the origin of the cause was hardly explored. A more detailed study was reported by Peng et al. [27] who made a comparative study of the electrochemical behaviours of different current collectors – Al foil, 2D graphene film, and 3D carbon nanotubes (CNT) – in Li–S batteries. Of the three collectors, only Al foil was commercially sourced; the others were synthesised by the authors. The best and worst current collectors were 3D CNTs and Al, respectively. The origin of poor current collection in Al was ascribed to the severe inhibition of electrochemical corrosion which occurs on the Al foil. This interpretation differs with the results obtained by Raguzin et al. [28] in a comparative study of different metallic current collectors (Al, Ni, Cu and Pt). The best results were obtained for Al and Pt. These elements were found to be the most inert collectors towards the cycle performance because of nonreactivity within the potential window (2.5-1.5 V). On the other hand, the macroscopic structure of 3D CNTs also plays an advantageous role in the cycling stability of the cell.

More recently, we have addressed a preliminary study on this topic by conducting a comparative study on two commercial current collectors: Al foil, the most commonly reported in the literature; and a gas diffusion layer (GDL), a carbon paper commonly used in fuel cells [29]. The performance of the cell made from the GDL collector was superior to that made with Al foil, due to the favourable surface morphology of GDL, its macroporous texture in particular. As a solution to the issues with Al foil as a current collector, manufacturers have introduced a modification consisting of a C layer coating, to improve chemical stability and texture, and achieve higher battery performance. In this contribution, we expand and complete the comparative study of the current collectors GDL, Al foil, and C-coated Al foil, the three commercial collectors commonly used in Li–S batteries. As the cathode, two C/S composites have been used, each with different carbon types and different methodologies for S impregnation. One of the carbons was a 3D N-doped graphene physically activated with CO_2, and impregnation with S was performed using the element dissolved in

ethylenediamine. The carbon host has a dual micro-mesoporous system, able to confine a high S content (~70%) and enhance both electrode impregnation by the electrolyte and the ability to trap polysulphides during the electrochemical process [30]. The other carbon was a commercial carbon black, used as a conductor. The S content was similar but impregnated into carbon by the commonly-used melt diffusion method.

2. Experimental

2.1 Composite and electrode preparation

Current collectors. Three types of commercial current collectors were tested in this study. Carbon cloth (GDL ELAT LT1400 W, 454 μm thick, Fuel Cells), Al foil (15 μm, MTI Corp.) and Al foil (20 μm) coated with a C layer on both sides (Custom Cells).

C/S composites. Two C/S composites were prepared, using different carbons and S impregnation methods. In the first composite, a 3D N-doped graphene was prepared from pristine graphite flakes, which were oxidised to graphitic oxide (GO) and further activated with CO_2. Sulfur was impregnated as nanoparticles, by dissolving the element in ethylenediamine [31]. The S composite is hereafter referred to as 3D-A-NG/S, and its S content was around 70%. Full descriptions of the graphene synthesis, its activation and composite preparation are given in previous reports [30,32]. In the second composite, a commercial carbon (carbon black, Super P, Timcal) was used, along with commercial micron-sized S (Solvay) in a 30:70 mass ratio. The mixture was milled inside the glovebox, loaded into a glass tube, tightly sealed and heated at 155 ºC for 24 h. This composite is hereafter referred to as CB/S, and its S content is as expected (near 70%), as confirmed by thermogravimetric data (see Fig. S1).

Electrode preparation. The electrodes were prepared by mixing composites with polyvinylidene fluoride (PVDF 6020, binder, Solvay) and Super P carbon (conducting agent, Timcal) in weight ratios of 80:10:10, with 1-methyl-2-pyrrolidone (NMP, Sigma Aldrich) used as the solvent. The resulting slurry was cast on the respective substrates through a doctor blade (MTI) method. The electrodes

were dried for 3 h at 50 °C using a hot plate and cut into disks 13 mm in diameter. The active material loading was between 1.8–2.3 and 1.4–1.8 mg cm^{-2}, for 3D-A-NG/S and CB/S composites, respectively.

2.2 *Characterisation techniques*

Structural properties were examined using X-ray diffraction (XRD) and X-ray photoelectron spectroscopy (XPS). The XRD patterns were recorded with a Bruker D8 Discover X-ray diffractometer, using Cu $K\alpha_1$ radiation and a Ge monochromator. XPS measurements were performed using a Physical Electronics spectrometer (PHI 5700) with non-monochromatic X-ray Mg $K\alpha$ radiation (720 μm diameter analysis area, 300 W, 15 kV, 1253.6 eV) as the excitation source. High-resolution spectra were recorded at a take-off angle of 45°, using a concentric hemispherical analyser operating in the constant pass energy mode at 29.5 eV. The spectrometer energy scale was calibrated using Cu $2p_{3/2}$, Ag $3d_{5/2}$, and Au $4f_{7/2}$ photoelectron lines at 932.7, 368.2 and 84.0 eV, respectively. Under these conditions, the Au $4f_{7/2}$ line was recorded with 0.73 eV full width at half maximum (FWHM). A PHI Smart Soft-VP 2.6.3.4 software package was used for data acquisition and analysis. Binding energy (BE) values were referenced to the C 1*s* peak at 284.8 eV. A Shirley-type background was subtracted from all signals. All recorded spectra were fitted using Gauss−Lorentz curves. Atomic concentration percentages of the characteristic surface elements were determined, considering the corresponding areas' sensitivity factors for the different measured spectral regions. An Ar^+ plasma gun was used at 4 kV for the etching process. For post-mortem studies, a cell with 3D-A-NG/S composite was chosen. After dismantling the cell inside the glove box, the electrode separated from the remaining components was cleaned by immersing it in ethanol, and after 5 min under ultrasound the surface was left with the typical appearance of Al. The dried electrodes were collected in an Eppendorf vessel and sealed for transfer to the XRD or XPS instrument.

SEM images were obtained with a JEOL JSM 7800F apparatus equipped with an X-max 150 microanalysis system. A mercury porosimeter (Autoscan-60 Quantachrome) was used for mercury

intrusion experiments. The values of surface tension and contact angle used in the computational program of the porosimeter were 0.480 N m^{-1} and 144º, respectively.

2.3 Symmetrical cells

Al foil, Al foil coated with C, and GDL were used as identical working and counter electrodes. The electrolyte composition used for the separator impregnation was 1 M LiTFSI, 0.4 M $LiNO_3$ dissolved in DOL: DME (v/v = 1/1), and 50 µL of Li_2S_6 were added. Polysulfide solution were prepared by mixing Li_2S and S with a molar ratio of 1:3 into a 1:1 (v/v) DOL/DME mixture, and stirred for 24 h at 60 °C. Cyclic voltammetry (CV) measurements were carried out at a scan rate of 5 mV s^{-1} between -1.0 V and 1.0 V.

2.4 Electrochemical measurements

Electrochemical experiments were performed on CR2032 coin cells assembled inside an Ar-filled glove box (M-Braun 150 model), with Li metal foil as both counter and reference electrode. The electrolyte was LiTFSI (1M, Sigma Aldrich), $LiNO_3$ (1M, Panreac) in 1,3-dioxolane (DOL, Sigma Aldrich) and 1,2-dimethoxyethane (DME, Sigma Aldrich) (1:1 v/v) impregnated in a polyethylene membrane (Celgard) as separator. The electrolyte volume used in all cells was 60 µL. Cyclic voltammetry (CV) measurements were performed at a scan rate of 0.1 mV s^{-1} within a 1.7–2.7 V range using Autolab PGSTAT-204 equipment. The same device was used for electrochemical impedance spectroscopy (EIS) measurements, performed in the frequency range of 500 kHz to 0.1 Hz at a disturbance amplitude of 10 mV. Galvanostatic cycling measurements were conducted in a voltage range of 1.8–2.6 V on an Arbin BT2143 battery test system. The specific capacity values were calculated based on the sulfur mass in the electrode.

3. Results and discussion

The galvanostatic charge-discharge profiles of the CB/S composite deposited on GDL, Al-C and Al foil collectors, at different cycles and at a current rate of 0.1C (1C = 1675 mA g^{-1}) recorded between 1.8–2.6 V, are shown in Fig. 1a and Fig. S2a and b. As expected, two well-defined discharge plateaus

appeared around 2.4 and 2.1 V, assigned to the S reduction to long- and short-chain polysulphides (including Li_2S), respectively, whereas the same plateaus are less defined (around 2.28 and 2.4 V) during the reverse oxidation reactions [33]. The origin of the sloping region below 1.9 V, only observed for the GDL collector, is unclear, and this region does not always appear [34]. Previous reports assigned this region to the precipitation of Li_2S_2 to Li_2S [35]. It is worth noting the notable influence that the current collector exerted on the capacity values supplied by the electrode. The first discharge capacity experienced a pronounced decrease when GDL (1525 mAh g^{-1}) was swapped for Al-based current collectors (1025 and 1075 mAh g^{-1} for Al-C and Al collectors, respectively). On charging the cell, the two plateaus observed in the discharge process appeared, showing the usual behaviour; that is, a strong polarisation, especially in the plateau associated with the formation of the insoluble, low order polysulphides (Li_2S_2, Li_2S). The sloping region of the discharge below 1.8 V disappeared, indicative of the irreversibility of the electrochemical process below 2.6 V (the upper limit imposed on cell cycling).

The variation of the specific capacity as a function of cycle number is shown in Fig. 1b. The pronounced drop in capacity in the first cycle is commonly observed, due to the period required for cell stabilisation. However, it is worth noting the much more pronounced drop of the Al-based electrodes. Since the S loading is like that based on GDL, and the other components of the electrodes, carbon black and binder, as well as the volume of the electrolyte, are equal, this difference must be attributed to the current collector and especially to its textural properties as we will discuss later. The capacity delivered by the GDL-based electrode after 250 cycles was 735 mAh g^{-1}, notably higher than that of Al-C and Al–based electrodes (365 and 300 mAh g^{-1}, respectively). Once the cell was stabilised, the three collectors provided Coulombic efficiency values of approximately 100%.

The rate capability measurements also showed the advantage of the GDL as a current collector, showing an increase as the current rate increased (Fig. 1c). In the discharge curve, the sloping region below 1.9 V was repeated, and disappeared when the cell was charged (Fig. S2a). The average capacity values of this electrode varied from 1130 mAh g^{-1} at C/10 to 500 mAh g^{-1} at 2C. When the

current rate was restored to C/10, the capacity increased to ca. 820 mAh g^{-1}, above 70% of the capacity corresponding to the star of the test. Al-based current collector cells only responded to low current rates, with 0.1 and 0.2C delivering average capacities of 475 and 350 mAh g^{-1} respectively, and the C coating had minimal influence on capacity. From 0.5C and upwards, the cell capacity was negligible. When the current rate was restored to C/10, the two cells recovered their activity, and the capacity of approximately 360 mAh g^{-1} is only 25% lower than the original value.

Other properties affected by the nature of the current collector were the voltage gap (ΔE) between the plateaus of the two stages in which the electrochemical process takes place. The calculated values from the charge-discharge profiles shown in Figs. 1a, S2a,b, and S3a,b,c are collected in Table 1. Independently of the current collector, polarisation increased in parallel with current density, as the reaction between Li and S was sluggish. Nevertheless, the Al-based electrodes exhibited much higher and faster voltage increase gaps. The values are especially high for both current collectors, likely the origin of the incapacity of the composite deposited on both substrates to operate at currents greater than 0.2C.

Table 1. ΔE values (V) calculated from the plateaus assigned to $S_8 \leftrightarrow Li_2S_n$ (n = 8, 6) and L_2S_n (n = 8, 6) $\leftrightarrow Li_2S_n$ (n = 2, 1) reversible transformations. Composite: CB/S.

Current collector	**Long term cycling (0.1 C)**		**Rate capability**	
	3rd cycle	**250th cycle**	**C/10**	**C/5***
	$S_8 \leftrightarrow Li_2S_n$ (n = 8, 6)			
GDL	0.04	0.03	0.03	0.06
Al-C	0.04	0.09	0.18	0.39
Al	0.08	0.10	0.19	0.39
	L_2S_n (n = 8, 6) $\leftrightarrow Li_2S_n$ (n = 2, 1)			
GDL	0.16	0.13	0.20	0.26
Al-C	0.18	0.27	0.31	0.56
Al	0.18	0.25	0.30	0.54

*The Al-based electrodes only operate below this value.

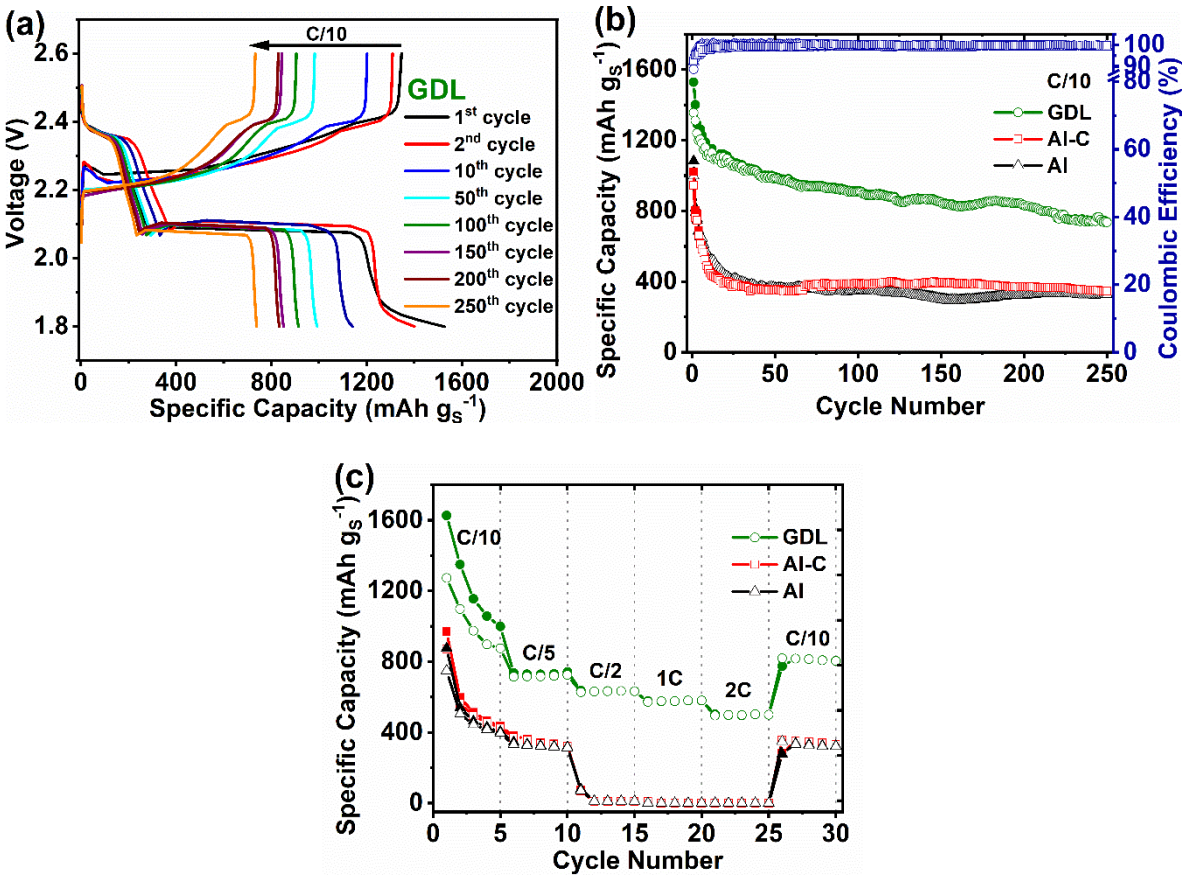

Fig. 1. Results of measurements carried out in the galvanic regime on the CB/S composite. (a) Discharge/charge curves recorded between 1.8–2.6 V at C/10 (1C = 1675 mA g^{-1}). (b) Discharge/charge specific capacity and coulombic efficiency values as a function of the cycle number. (c) Rate capability tests.

The capacity values of the electrodes discussed in Fig. 1 were calculated considering only their S content. Since GDL is a source of carbon, its contribution to the performance of the cell could raise doubts about the reliability of the above results. To clarify this dilemma, we have studied a new electrode with a sulfur loading of 2 mg cm^{-2} using the same ratios of its three components and evaluating the normalised capacity with respect to the entire electrode weight (S, CB, PVDF and current collector). The capacity values plotted as a function of the number of cycles, Fig. S4, confirm the best performance of the electrode with GDL as a current collector, although, as expected, the capacity values are different.

To ensure that the differences in the electrode performance were due to the nature of the current collector and the composite, and that their preparation plays a minor role, a similar study was

conducted using the 3D-A-NG/S composite, of which the carbon component and the S impregnation method are completely different to that of the CB/S composite. To eliminate the side reaction below 1.9 V observed for the GDL collector, the galvanostatic study was carried out between 1.9–2.6 V. In addition, long term cycling measurements were performed at a higher speed (C/5). The shape of the curves (Fig. 2a and Figs. S5a, b) was the same as that for the CB/S composite. The differences affect the capacities delivered by the electrodes, as well as the polarisation values between the charge/discharge curves, in addition to the almost negligible plateau below 1.9 V for the GDL-based electrode.

Although the initial capacities were lower than those obtained for the CB/S composite (1314 mAh g^{-1} for GDL and 803 and 960 mAh g^{-1} for Al-C and Al collectors, respectively), the decrease in capacity during cycling was less pronounced (Fig. 2b), and the capacity values at 250 cycles clearly exceed those of the CB/S composite for the three collectors: 850, 506 and 448 mAh g^{-1} for GDL, Al-C and Al, respectively. It is worth noting that these data were recorded at twice the current rate, making the performance improvement of this electrode even more impressive. Although the aim of this study was not to delve into the cause of differences in the performances of each composite, we believe that the S impregnation method and the greater pore volume of graphene were the main factors responsible for the observed improvement in performance [31,36,37]. For the purpose of this study, the same pattern is observed in terms of current collector performance. The superior behaviour of the GDL electrode was again clearly observed, as well as the minimal differences between coating or not coating the Al substrate with C.

The rate capability measurements confirmed the optimal properties of GDL as a current collector, and its performance even increased at higher current rates (Fig. 2c). The average capacity values of the GDL-based electrode varied from 1404 mAh g^{-1} at C/10 to 994 mAh g^{-1} at 2C, a remarkably high value, considering the elevated current rate. When the current rate is restored to C/10, the capacity loss was only 15%. In contrast, the capacity of the cell with an Al-C current collector decayed to 761 and 220 mAh g^{-1} at C/10 and 1C, respectively. At 2C, the capacity was negligible. Al foil decays

even further; at C/10, the average capacity decreases to 634 mAh g^{-1} and becomes negligible at 1C. As in the measurements carried out during long-term cycling, the differences between the current collectors based on Al were small, and the improvement of electrode performance provided by the C coating was low. In these measurements, the superior electrochemical behavior of the 3D-A-NG/S composite compared to that of the CB/S becomes even more pronounced. The nanometric size of the S particles is likely to facilitate reaction kinetics, and the composite can respond to higher values of current rates regardless of the substrate used.

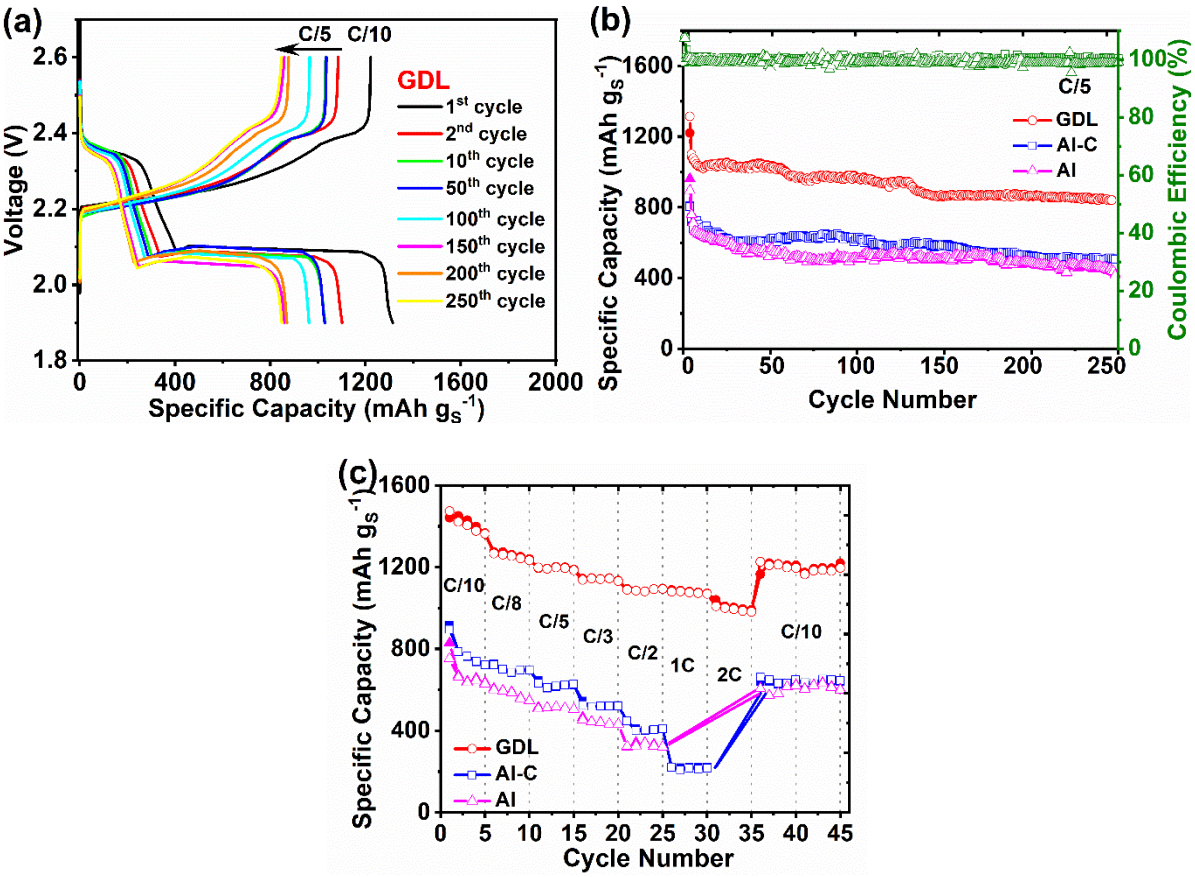

Fig. 2. Results of measurements carried out in the galvanic regime on the 3D-A-NG/S composite. (a) Discharge/charge curves recorded between 1.9–2.6 V at C/5. (b) Discharge/charge specific capacity and Coulombic efficiency values as a function of cycle number. (c) Rate capability tests.

The voltage gap (ΔE) values between the plateaus describing the two electrochemical processes calculated from the charge-discharge profiles of 3D-A-NG/S, shown in Fig. 2a, Fig. S5a,b and Fig. S6a,b,c, are collected in Table 2. The values showed a sequence like that observed for the CB/S

composite (Table 1). Thus, the Al-based electrodes displayed higher values than those of the GDL electrode. However, the polarisation observed in this composite was lower. Note that: for the Al foil collector, polarisation could be measured for current up to C/2; for the Al-C collector, up to 1C; and for the GDL collector, up to 2C. These lower polarisation values and lower electrode resistances are responsible for the higher capacity values delivered by the composite.

Table 2. ΔE values (V) calculated from the plateaus assigned to $S_8 \leftrightarrow Li_2S_n$ (n = 8, 6) and L_2S_n (n = 8, 6) $\leftrightarrow Li_2S_n$ (n = 2, 1) reversible transformations. Composite: 3D-A-NG/S. (*1C)

Current collector	Long term cycling (0.2 C)		Rate capability		
	3rd cycle	250th cycle	C/10	C/2	2 C
	$S_8 \leftrightarrow Li_2S_n$ (n = 8, 6)				
GDL	0.04	0.1	0.02	0.07	0.23
Al-C	0.06	0.15	0.11	0.31	0.66*
Al	0.15	0.2	0.07	0.58	-
	L_2S_n (n = 8, 6) $\leftrightarrow Li_2S_n$ (n = 2, 1)				
GDL	0.16	0.23	0.13	0.19	0.43
Al-C	0.16	0.40	0.24	0.48	0.58*
Al	0.28	0.36	0.26	0.70	-

Considering the superior electrochemical properties of this composite, more thorough characterisation was performed by measuring its behaviour in cyclic voltammetry (CV), and, in parallel, a study of its impedance spectra was also performed. For the GDL current collector, both measurements were previously reported elsewhere [30]. The CV curves of the Al-C and Al collectors are shown in Fig. 3, together with those of GDL for ease of comparison. The shape was the expected two peaks for the reduction scan, and another asymmetric peak for the oxidation scan, consistent with the plateaus discussed for the galvanostatic discharge and charge curves [38]. It is worth noting the small broadening of the GDL collector peaks compared to that of the Al-C and Al collectors. In fact, the asymmetry of the oxidation peak is barely perceptible. These results reveal the superior kinetic

properties of the composite deposited in the GDL collector towards the Li reaction and are in good agreement with the previously discussed results from galvanic measurements.

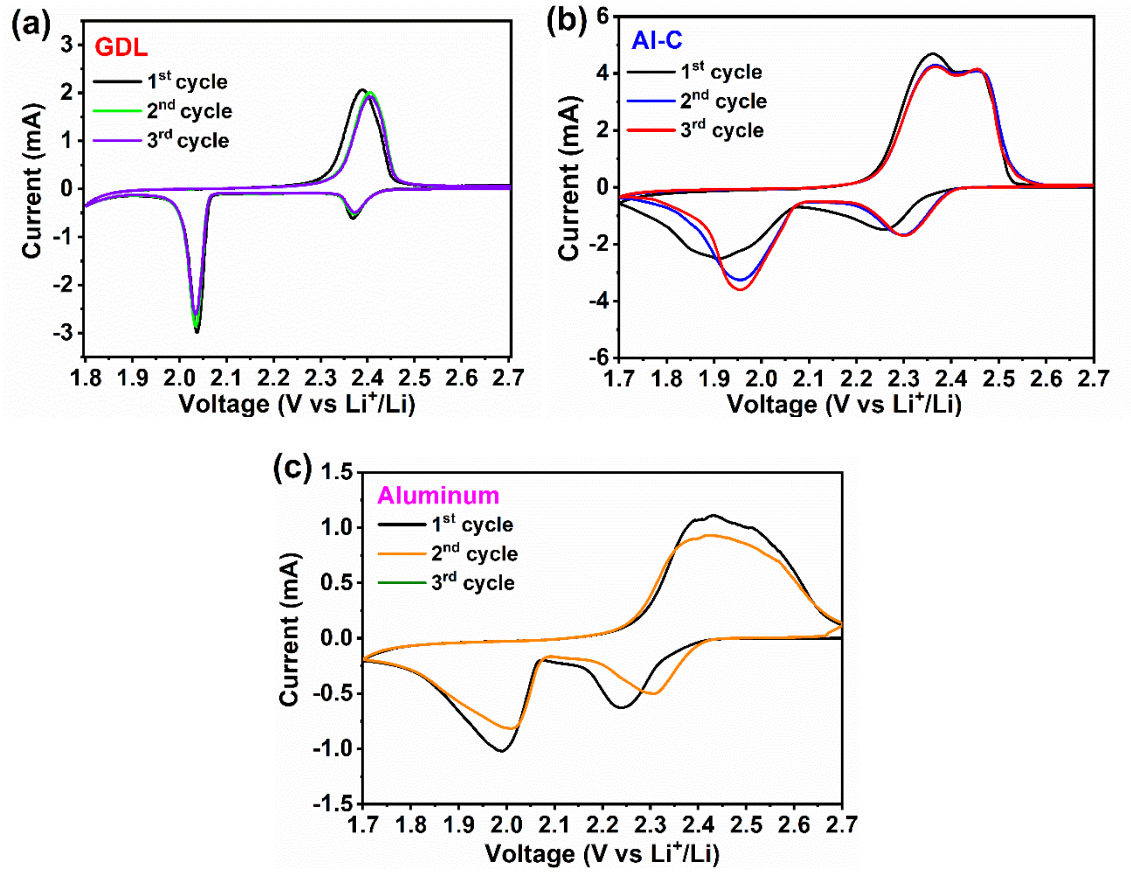

Fig. 3. Cyclic voltammetry curves for the 3D-A-NG/S composite, recorded at 0.1 mV s^{-1}. (a) GDL, (b) Al-C, and (c) Al collectors.

The impedance curves are shown in Fig. 4, and the results of the equivalent circuits in Table 3. At high frequencies, they intercept on the real axis at the electrolyte resistance (R_e), followed by semicircles in the high-to-medium frequency region, related to the electrode/electrolyte interphase, including resistances of both the charge transfer (R_{ct}) and the solid electrolyte interphase (SEI) film formed at the electrode surfaces [39]. The inclined line in the low frequency region is related to Li^+ diffusion in the electrode (Warburg impedance). The effect exerted by cycling the electrode was independent of the nature of the current collector, shown by a decrease of the electrode/electrolyte interphase resistance, associated with a reorganisation of the electrode material during cycling [40].

In open circuit voltage (OCV), the highest resistance values were presented by the Al collector, which almost exceeded 200 Ω, followed by the Al-C (77 Ω) and the GDL (28 Ω). After cycling, the calculated resistance values for Al, Al-C and GDL were 88, 12 and 22 Ω, respectively. Although the GDL electrode exhibits the best performance, it does not have the lowest impedance values. Therefore, it does not appear that this property is the main responsible for the activity of the electrode. In fact, significant differences are also observed in the impedance values for the Al-C and Al electrodes. However, these differences are not reflected in the values of the specific capacities, similar in both electrodes (Figs. 1, 2).

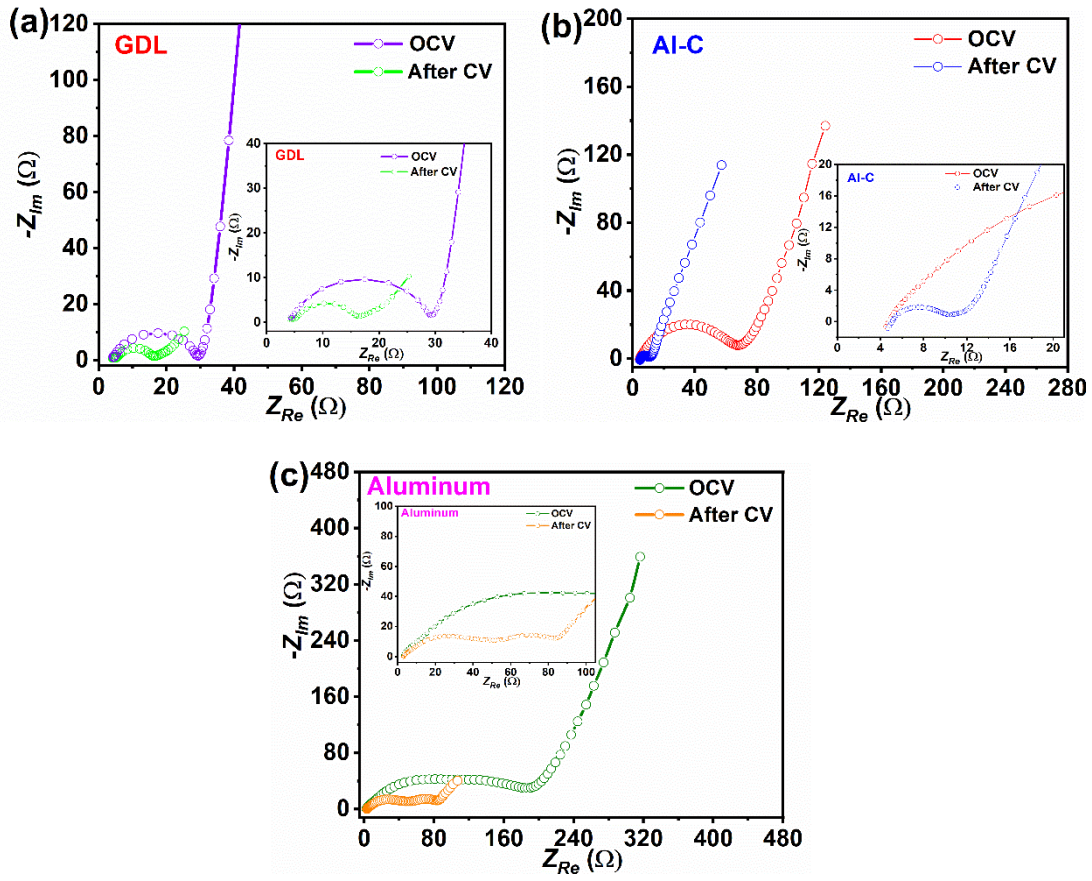

Fig. 4. EIS curves before and after recording CV curves. (a) GDL, (b) Al-C, and (c) Al collectors; and insets show magnifications of each experiment: (a) GDL, (b) Al-C, and (c) Al collectors.

Table 3. Calculated resistances of the impedance spectra of the electrodes made from 3D-A-NG/S composite. The spectra were recorded upon cyclic voltammetry (Fig. 3).

Collector	Cell condition	Circuit	R_e (Ω)	R_1 (Ω)	R_2 (Ω)	R_3 (Ω)	$R_T = R_1 + R_2 + R_3$ (Ω)
GDL	OCV	$R_e(R_1Q_1)\ (R_2Q_2)Q_g$	4.2	25.3	2.5	-	27.8
	After 3 cycles	$R_e(R_1Q_1)\ (R_2Q_2)\ (R_3Q_3)Q_g$	4.1	3.0	10.1	8.8	21.9
Al-C	OCV	$R_e(R_1Q_1)\ (R_2Q_2)Q_g$	4.5	66.6	10.0	-	76.6
	After 3 cycles	$R_e(R_1Q_1)\ (R_2Q_2)Q_g$	4.6	6.7	5.5	-	12.2
Al	OCV	$R_e(R_1Q_1)\ (R_2Q_2)Q_g$	2.9	95.4	98.1	-	193.5
	After 3 cycles	$R_e(R_1Q_1)\ (R_2Q_2)Q_g$	3.0	40.8	46.3	-	87.1

To shed additional light on the kinetics of the electrochemical reaction, the CV curves of symmetrical cells were recorded, Fig. 5 a,b. Two observations should be noted. First, clear differences in the polarisation profiles resulting from Li_2S_6 redox and capacitive currents are observed. While for the Al foil, Al foil coated with C collectors, and for the GDL collector without Li_2S_6, the small current density is, due to the capacitive component; and for the GDL collector with Li_2S_6 the polarisation curve is directly related to the redox current of lithium polysulfide. If we compare the current densities of both figures, an increase of an order of magnitude is observed in the cell with the GDL as the electrode (Fig. 5b). Furthermore, the CV curve of this cell exhibits broad redox peaks reminiscent of the characteristic peaks of the reaction between Li and S, Fig. 4. These results agree with the polarisation values between the galvanostatic charge/discharge curves and confirm the role of the GDL collector in accelerating the redox process. In some way, GDL itself acts as a catalyst for the LiPS conversion as observed in other chemical species such as CoS_2 [41], Ir [42], MoS_2 [43] and VO_2(P) [44].

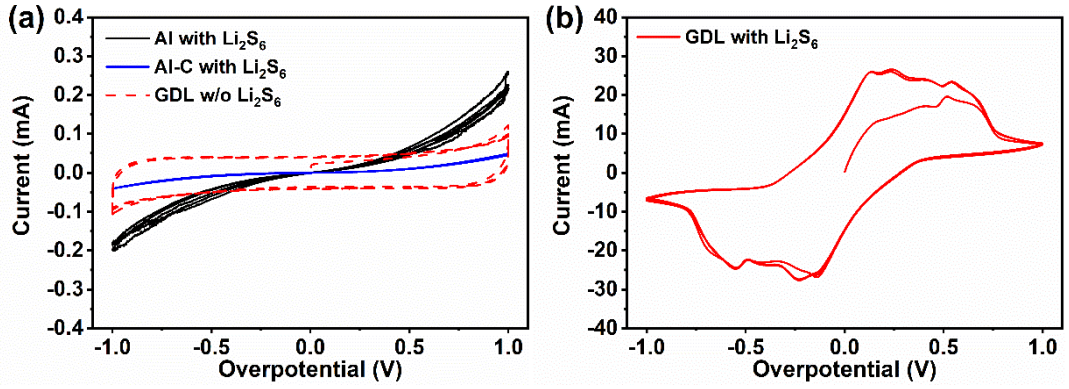

Fig. 5. Polarisation curves of symmetrical cells made from current collector electrodes with and without Li_2S_6.

The electrochemical corrosion of Al has been suggested as one of the reasons for the deterioration of Li–S batteries, due to its direct contact with the electrolyte and S, and to the electrochemical reaction itself. It has been proposed that Al can react with S directly, forming Al_2S_3, but high temperatures are required [45]. The corrosion of Al in electrolyte solutions of $LiN(CF_3SO_2)_2$ has been studied by Yang et al. [46]. Oxidation takes place at voltages higher than 3.5 V, much higher than the cut-off potential used in this study (2.6 V). These observations are consistent with the XRD patterns of the Al collector before and after cycling (Fig. 6). The formation of phases other than Al was not observed on either side of the electrode (the peak located at around $2\theta = 26^{o}$ is due to the Mylar protective film used to record the diffractogram). It is well known that microstructure and thickness affect the intensity of the polycrystalline Al foil peaks, hence the low intensity of the (111) and (200) planes [47,48]. In addition, the Al foil coated with carbon has a very similar XRD pattern (Fig. S7), due to originating from the same manufacturer. In this case, there were no peaks other than those of Al. No peaks assignable to species such as $Li(OH)\cdot 2H_2O$ or $LiAl_2O_7\cdot 2H_2O$, as reported by Peng et al. [27], were found – the latter compound is, in fact, unknown, as it does not conform to the elementary valences of the elements. The oxidation of Al in Li–S batteries has also been tackled by Li et al. [49], combining electrochemical measurements with data obtained from synchrotron-based X-ray absorption near-edge spectroscopy (XANES). These authors suggest the formation of Al^{3+} species in the form of AlF_3, although the spectroscopic data provided are unconvincing since the spectra recorded before and after cycling the electrode are practically identical. On the other hand, from chemical considerations, the AlF_3 formation would be difficult since the F source comes either from the electrolyte, LiTFSI, or from the additive, PVDF-HFP (poly(vinylidene fluoride-co-hexafluoropropylene)) used in the preparation of the electrode. In both cases F is bound to C by strong covalent bonds making it difficult to find plausible ways for the formation of an ionic compound such as AlF_3.

On the other hand, no peaks assignable to Li_2S_n (n = 1, 2) from the cell discharge were identified. This is due to the protective film used, whose intense peak located around $2\theta = 26^o$ makes it difficult to identify the broad, low-intensity peak observed around $2\theta = 27^o$, assigned to Li_2S, when the diffractogram of the cell is recorded either *in-situ* [50] or *ex-situ* [51]. When the XRD pattern of the cycled electrode is recorded without the protection of the Mylar film, the only peaks clearly detected, aside from those of Al, are those of S, consistent with the state of charge in which the cycling process has been cut (Fig. S7). Therefore, no peaks from Al corrosion products were identified in this study, raising a question about the Al corrosion caused by the electrolyte, or by the electrochemical reactions that take place during the cell's charge and discharge processes. Our results are more in agreement with the conclusion of Raguzin et al. [28] on the reluctance of Al to undergo electrochemical reactions during the cycling of Li–S batteries, providing experimental evidence.

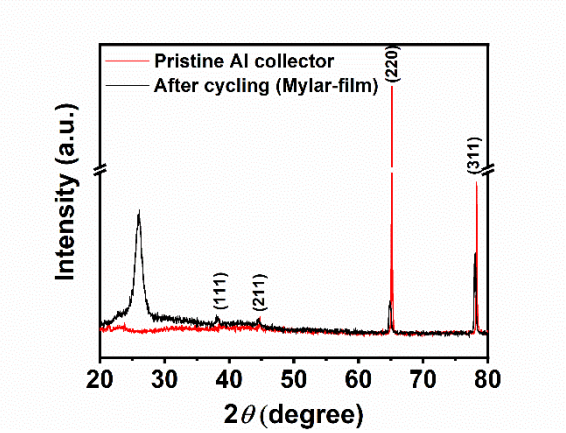

Fig. 6. XRD pattern of the pristine Al collector and the electrode after cycling (under the protection of Mylar protective film). The disc was exposed to the radiation on the active material side.

The electrical conductivity of the collector is another property to consider with regard to electrode performance. Better electrochemical properties would be expected as a result of increasing the electrical conductivity. The absolute values found for conductivity are quite contradictory with each other, as shown in Table 4. We do not have a satisfactory explanation for these differences, as there are several factors which affect conductivity measurements, such as foil thickness [52]. Aside from

the absolute values, some comparisons can be made between the three collectors. As expected, Al-based collectors have significantly higher conductivity than C-based (GDL); in addition, coating with C slightly increases conductivity. The higher conductivity of the current collector and lower internal resistivity of the cell do not explain the improved electrochemical properties of the GDL collector, as it has the highest resistivity values.

Table 4. Electrical resistivity values of current collectors (in Ω·cm).

Collector	Commercial	This work	Ref. [53]
Al	$2.05 \cdot 10^{-6}$	$2.5 \cdot 10^{-3}$	28.1
Al-C	-	$1.8 \cdot 10^{-3}$	14.3
GDL	$3.5 \cdot 10^{-3}$	3.5	-

Other properties which directly affect the electrochemical response of the collectors are the structure and texture of their surfaces, and analysis of these can shed light on the differences observed in the electrochemical behaviour of the electrodes. These properties were analysed using three different techniques: SEM, XPS and Hg porosimetry.

The microstructures of the current collectors, revealed by SEM images, are shown in Fig. S8. The Al surface is quite smooth, and exhibits straight grooves originating from the manufacturing process. On the other hand, the C coating of the Al-C collector is inhomogeneous, with areas covered by microparticles with different morphologies, and other areas appearing uncoated. Hence, the manufacturer's estimated C coating thickness of 2 μm is questionable. The microstructure of the GDL support is quite different, exhibiting severe roughness with multiple micrometric fractures, in both its width and depth. These cavities can more efficiently anchor the active slurry material in the collector. This phenomenon is clearer from cross-sectional images as shown in Fig. S9. Al and Al-C images show the expected features, with smooth surfaces with occasional bumps due to lack of polishing. By contrast, the GDL images clearly reveal the macroporous nature of the deposited C layer, formed with

particles of different morphology, pseudo-cottony lumps dominating the top side, and carbon fibers at the back side, to maintain the deposit integrity.

The XPS survey spectra of the three collectors are shown in Fig. S10, and the identified element contents in Table 4. The following observations should be noted, (i) C and O were identified in all three collectors, (ii) Al was not detected in the Al-C survey spectrum, and (iii) the GDL collector has a high F content.

Table 5. Chemical composition (in atomic concentration [%]) of the collector surfaces, calculated from the XPS survey spectra.

Collector	C	O	Al	N	F
Al[+]	56.9	28.8	12.0	1.2	-
Al-C	67.5	29.1	-	3.3	-
GDL	50.6	1.2	-	-	48.2
Al[*]	47.6	35.9	13.8	-	-

[+] This collector has a small Si content (0.9%). [*] Al foil after 250 cycles: Si content (2.4%)

Another significant observation concerns the shape of the Al 2*p* photoemission peak, which has two components at BE values of 71.4 and 74.3 eV, with the intensity of the latter being much higher (Fig. 7a). These values are consistent with two chemical environments for the element: the Al itself, and Al bound to oxygen as Al_2O_3, respectively [54]. This implies that the Al is coated with an oxide layer, the thickness of which was estimated from XPS depth profile analysis. The evolution of the Al 2*p* signal with sputtering time is shown in Fig. 7b. The intensity of the high- and low-BE components decrease and increase, respectively, with sputtering time. For comparison, we have included in Figs. S11a and b the evolution of the C 1*s* and O 1*s* peaks with sputtering time. As can be seen, the C 1*s* peak disappears after the first few minutes of sputtering, characteristic of adventitious carbon. In contrast, the disappearance of the O 1*s* peak is much slower, and even after 14 min of sputtering is

still perceptible. The evolution of the atomic concentration of C, O, Al^{3+} and Al^0 is shown in Fig. 7c. These data can be used to approximately calculate the thickness of Al_2O_3 coating. After 6 min of etching, a drastic reduction in the intensity of the O peak and that associated with Al^{3+} occurs. Considering an etching rate of 5 nm/min for SiO_2, and that the relative etch rate for Al_2O_3 is 2.0 nm/min [55], the thickness of the Al_2O_3 barely exceeds 30 nm, which is too low to significantly affect the collector conductivity. This insulating coating may affect more the interface between the active material and the substrate, reflected in the higher impedance values of this electrode (Table 3).

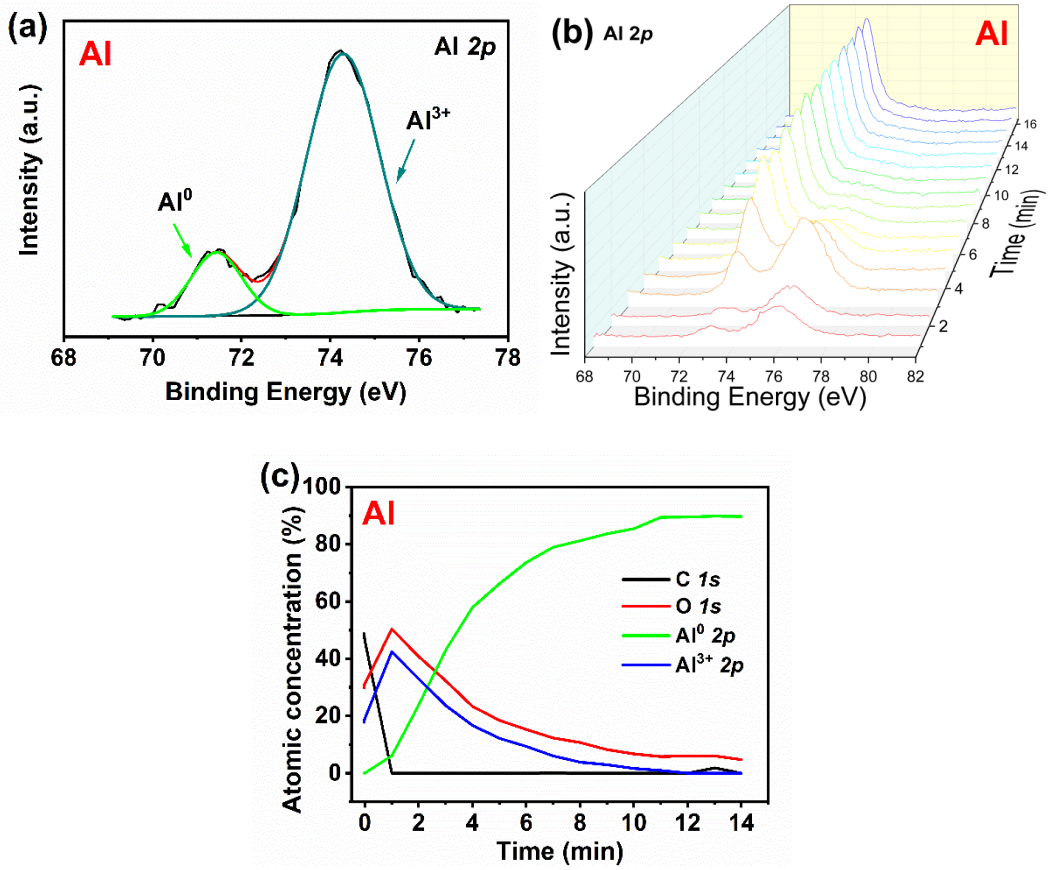

Fig. 7. Al 2*p* photoemission peak of Al collector (a) and depth profiles spectra (b). Evolution of the atomic concentration as a function of the sputter time with Ar^+ (c).

The absence of the Al peak in the Al-C collector was caused by the coating with C. To detect Al, it was necessary to perform material sputtering. After approximately 6 min, the Al 2*p* signal began to appear (Fig. S12a). The first peak that developed was located around 74.3 eV, assignable to Al^{3+}. As the sputtering time increased, the localised peak at the lowest energy, assignable to Al metal, began

to appear. This peak became more intense after 13 min of sputtering. The C 1*s* signal (Fig. S12b) can be fitted to three components, with binding energies 286.4 (64.7%), 286.2 (19.8%) and 288.5 (15.5%) eV, assignable to C-C bonds, alcoholic or etheric (C-OH, C-O-C) and carboxyl (COO^-) groups, respectively [56]. These O-based functional groups disappeared in the first doses of Ar^+ treatment (Fig. S12c). Furthermore, the binding energy changed slightly, likely due to the C layer eliminated by the Ar^+ treatment corresponding to adventitious C and the signal observed in subsequent spectra corresponding to the C collector. Unlike the Al collector (Fig. 6c) C was the majority element during treatment (Fig. 12d), followed by Al, as the treatment time increased. At the end of the test, C and Al were the only two elements present, the latter near-entirely in metal form. These results shed additional light on the SEM analyses (Fig. S8b). The surface of Al was coated with C; although, the layer thickness is not homogeneous. Most C is deposited randomly, causing the somewhat rough appearance seen in the image.

The high F content found on the surface of GDL was surprising (see Table 5). The origin of the element lies in the treatment of the collector with PTFE during its manufacturing process. The C 1*s* photoemission signal (Fig. S13a) was resolved as four peaks, with BE = 284.4 (65%), 285.6 (10%), 286.7 (3.3%) and 292.0 (22%) eV. The second and third components are assigned to O-based functional groups, and the last component to the $-CF_2$ group present in the PTFE structure [57]. The F 1*s* photoemission peak (Fig. S13b) is somewhat asymmetric, and the maximum observed peak is located at 689.7 eV, which is slightly higher than that previously reported [57]. The origin of the peak appearing at 292.0 eV is unclear. In PTFE-based membranes, a similar signal is detected, and assigned to F-containing groups such as OCF [58]. We believe that the PTFE in GDL does not show these groups; although, we do not rule out that its origin is a consequence of differences in conductivity in the sample itself [59]. The depth profiles of C and F are shown in Fig. S14a and b, respectively. In both cases, a similar evolution of the signals involving F was observed: specifically, a drastic decrease in the intensity of the component associated with the CF_2 group and of the F 1*s* photoemission peak after the beginning of Ar^+ treatment. The evolution in concentrations of the elements detected, C, F

and O, the latter present in very little quantity, is shown in Fig. S14c. The first pickling induced a significant decrease in F, the level of which stabilised at around 20% at the end of the treatment. The rest is near-entirely C. Nevertheless, the high content of F in the collector may have a positive effect to trap polysulphides due to its high electronegativity [60]. Despite the clear F 1*s* photoemission peak after 14 min of sputtering (Fig. S15a), the intensity of the signal assignable to the -CF_2 group significantly decreased (Fig. S15b). The F 1*s* signal became more complex when a new lower-energy component appeared (Fig. S15c), suggesting chemical changes in F caused by the sputtering process. As there is no accurate data on the PTFE amount in the GDL collector, it is difficult to convincingly explain the observed changes.

The XPS technique can also be used as a tool to analyse the possible corrosion of Al caused by the electrochemical reactions undergone by the electrode. The composition analysis of the Al film by means of the depth profiles can shed light on the degree of Al oxidation, or the formation of other compounds considering the identified elements. The survey spectrum of the Al foil after being cycled for 250 cycles is shown in Fig. S16, and the elemental concentration in Table 5. Regarding the contents, the most notable was an increase in N and O, more pronounced in the latter, and a decrease in C. It is worth highlighting the absence of F from the electrolyte and consequently, the formation of species such as AlF_3 suggested by Li et al. [49], which supports our opinion regarding the difficulty of breaking C-F bonds in the electrochemical process. Nor was the presence of S detected, so the formation of $Al_2 S_3$ is ruled out. The profile of the Al 2*p* peak, Fig. 8a, and its evolution with sputtering time, Fig. 7b; is similar to that of the pristine Al foil, Figs. 7a, and b, two components at 71. and 74. eV, with a clear predominance of the highest energy associated with Al^{3+} at the first doses followed by the increase of the low-BE component associated to Al^0 and predominant in the last doses of etching. The evolution of the atomic concentration of C, O, Al^{3+} and Al^0 is shown in Fig. 8c. Applying the previous criteria for the evaluation of the Al_2O_3 layer thickness in pristine Al foil, the calculated value would be very similar. These results support that the electrochemical reactions and the

electrolyte hardly promote the Al corrosion. Hence, the thinness of the Al_2O_3 film could be the cause of being undetectable by XRD.

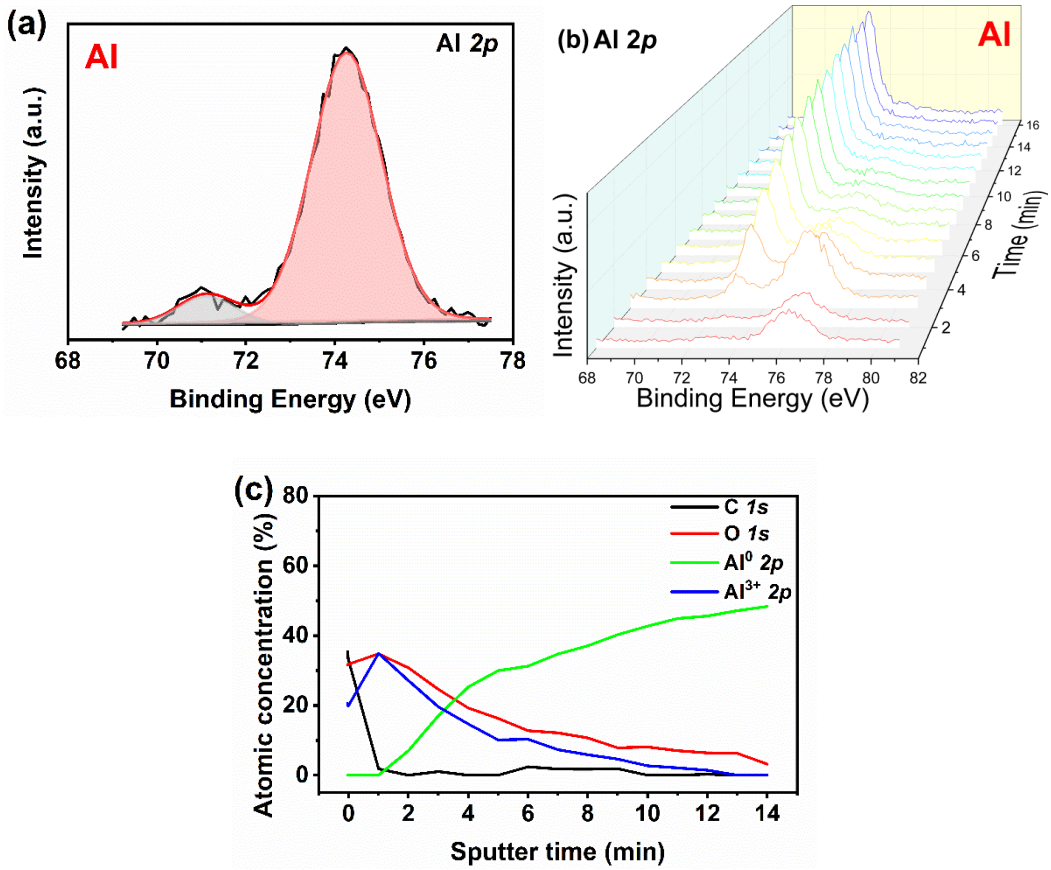

Fig. 8. Al 2*p* photoemission peak of Al collector after being cycled for 250 cycles at 0.2C (a) and depth profiles spectra (b). Evolution of the atomic concentration as a function of the sputter time with Ar^+ (c).

The porosity of the collectors was examined using Hg porosimetry, as the foils' smoothness, particularly for Al and Al-C, make N_2 adsorption measurements unfeasible. The pore cumulative volume (V_{cu}) vs. pore radius (r) are shown in Fig. 9a. Macropore (V_{ma}) and mesopore (V_{me}) volumes were calculated as $V_{ma} = V_{cu}$ (at r = 250 Å) and $V_{me} = V_{cu}$ (at r < 20 Å) – V_{ma} [61]. The calculated values of V_{ma} and V_{me} are shown in Table 6. In all three collectors, most of the cumulative porosity by volume is associated with V_{ma}; hence, the V_{me} values obtained are at the detection limit of the technique, implying that their role in the behavior of the electrode is, effectively, irrelevant. By comparison, the differences in V_{ma} values are remarkable. It should be noted that, (i) for Al, the V_{ma}

value was almost at the detection limit of the technique, 0.0003 cm^3 g^{-1} with the carbon coating causing a barely significant increase to 0.0032 cm^3 g^{-1}, and (ii) a spectacular increase in V_{ma} was observed for the GDL collector, almost 0.3 cm^3 g^{-1}, a 100-fold increase compared to the Al-C collector. The pore size distributions between 0.01 and 6 μm are shown in Fig. 9b. For Al-based collectors, only the Al-C exhibited the peak around 1 μm, assignable to the pseudo-C islands observed in the SEM image (Fig. S8). Its low intensity suggests its irrelevance in the electrochemical properties of the electrode. The pore-size distribution plot for the GDL collector showed greater complexity and more intense peaks (to be expected, considering the values of V_{cu}) (Fig. 9a). Three peaks near 0.03, 0.25 and 4 μm were identified. Although the latter size represents the predominant pore system of the collector, caused by the fractures shown in the SEM images (Figs. S8, S9), the presence of smaller pores may also contribute to improving impregnation of the electrode by the electrolyte. The combined effect of this dual system of meso- and macro-pores, absent in the Al and Al-C collectors, may benefit the kinetics of the reaction between Li and S by strengthening the electrode/electrolyte interface, key for good development of the charge-transfer-electron phenomena. The cycling properties (Figs. 1b, c and 2b, c), as a reference point for the electrochemical behavior of the electrodes, confirm this hypothesis, irrespective of the nature of the composite.

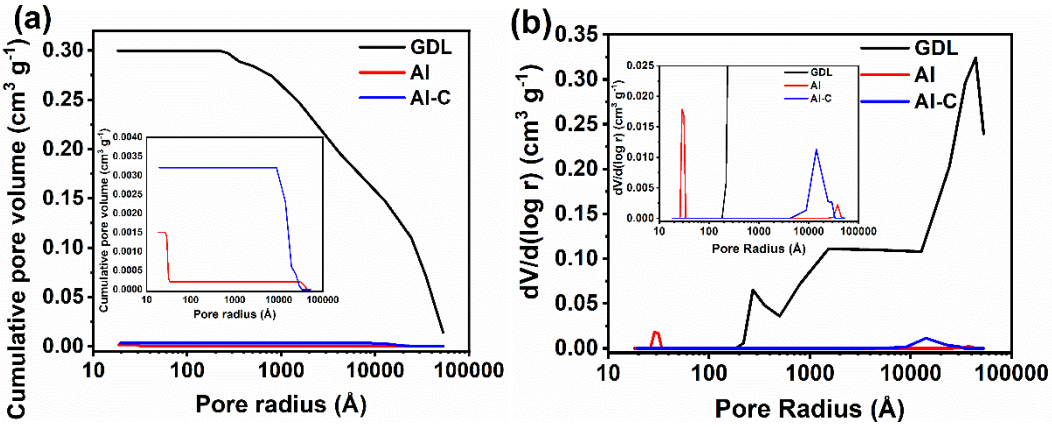

Fig. 9. Variation of the cumulative pore volume with the pore radius (a), and pore-size distribution (PSD) curve (b), for Al, Al-C and GDL current collectors; and insets show magnifications.

Table 6. Macro- and meso-pore volumes of current collectors (in $cm^3\ g^{-1}$).

Collector	V_{ma}	V_{me}
Al	0.0003	0.0002
Al-C	0.0032	0.0002
GDL	0.298	0.0013

The electrochemical results of the electrode with Al-C current collector deserves a special comment. The purpose of coating Al with a C layer has several motivations such as alleviating the stiffness of the metal and facilitating contact with the active particles of the electrode. This action should be reflected in a clear improvement in the performance of the electrode. Unfortunately, this improvement is hardly perceptible in the results obtained here. This behaviour differs with that found when the Al foil coating is carried out with other carbonaceous materials such as carbon nanotubes [62], graphene powder [63], or mixtures of both [64]. These non-commercial coatings are able to increase the electrode performance. We believe that the textural properties of the carbons used for the coating are responsible for the differences in the electrochemical responses of the electrodes. In our case, the C which covers Al lacks a hierarchical pore structure, as revealed by the Hg porosimetry data. The SEM images themselves show smooth, low surface area particles. On the contrary, in non-commercial carbons used to cover the Al foil, micropores and mesopores coexist and have high surface area and pore volume [63]. These textural properties provide not only space for the dispersion and anchoring of S and the polysulfides adsorption, but also facilitate the impregnation by the electrolyte together with the presence of adequate channels for the mobility of the current carriers, all beneficial aspects for the electrochemical reaction.

4. Conclusions

Although a battery's electrode current collector does not participate directly in the electrochemical reactions taking place, the role it plays can still affect battery performance. This was the main

conclusion of this work, which examined the three commercial current collectors commonly used in basic research of Li–S batteries: Al foil, Al-C foil and GDL. The GDL collector gave clearly superior results in all electrochemical measurements, while the differences in behaviour between the Al and Al-C collectors were minimal, within the experimental error of the measurements.

To explain these observations, different factors were analysed: corrosion of Al, surface composition, and the textural properties of the collectors, among others. XRD measurements obtained from post-mortem electrodes did not show the formation of species expected from corrosion of Al. XPS analysis of the collector surface composition, including depth profile measurements, revealed the presence of a very thin Al_2O_3 insulating layer in the pristine Al foil, of few-nm thickness. After cycling the electrode for 250th cycles the thickness of the Al foil hardly changes, indicating that the corrosion suffered has been insignificant. Regarding the C coating of the Al-C collector, the combination of depth profile measurements and SEM images revealed that it is inhomogeneous, as most of the C appears dispersed on the Al surface.

Hg porosimetry data were more enlightening in explaining the performance of the electrodes using each of the three current collectors. The GDL collector exhibited a pore volume significantly higher than that of the Al-based collectors in addition to a hierarchical meso- and macro-pore system, the latter being predominant. The presence of this pore system improves electrolyte impregnation of the electrode, so accelerating the kinetics of the reaction between Li and S by strengthening the electrode/electrolyte interface, key for good development of the charge-transfer phenomena. Al-based collectors, despite having higher electronic conductivities, lack this pore system. The electrochemical reaction slows down, causing a greater polarisation between the charge and discharge curves, which leads to a pronounced loss of electrode capacity.

Acknowledgments

This work was supported by Ministerio de Economía y Competitividad (Project MAT2017-87541-R) and Junta de Andalucía (Group FQM-175). A. Benítez thanks the financial support from Cordoba

University (Plan Propio de Investigacion 2019; Sub. 2.4.). E. Rodríguez-Castellón thanks to project RTI2018-099668-BC22 of Ministerio de Ciencia, Innovación y Universidades and FEDER funds.

References

[1] Y. Yang, M.T. McDowell, A. Jackson, J.J. Cha, S.S. Hong, Y. Cui, Nano Lett. 10 (2010) 1486–1491.

[2] N.-S. Choi, Z. Chen, S.A. Freunberger, X. Ji, Y.-K. Sun, K. Amine, G. Yushin, L.F. Nazar, J. Cho, P.G. Bruce, Angew. Chemie Int. Ed. 51 (2012) 9994–10024.

[3] N. Nitta, F. Wu, J.T. Lee, G. Yushin, Mater. Today 18 (2015) 252–264.

[4] P.G. Bruce, S.A. Freunberger, L.J. Hardwick, J.-M. Tarascon, Nat. Mater. 11 (2012) 19–29.

[5] X. Ji, L.F. Nazar, J. Mater. Chem. 20 (2010) 9821.

[6] M. Barghamadi, A. Kapoor, C. Wen, J. Electrochem. Soc. 160 (2013) A1256–A1263.

[7] D.-W. Wang, Q. Zeng, G. Zhou, L. Yin, F. Li, H.-M. Cheng, I.R. Gentle, G.Q.M. Lu, J. Mater. Chem. A 1 (2013) 9382.

[8] M. Rana, B. Luo, M.R. Kaiser, I. Gentle, R. Knibbe, J. Energy Chem. 42 (2020) 195–209.

[9] X. Hong, R. Wang, Y. Liu, J. Fu, J. Liang, S. Dou, J. Energy Chem. (2020).

[10] A. Manthiram, Y. Fu, S.-H. Chung, C. Zu, Y.-S. Su, Chem. Rev. 114 (2014) 11751–11787.

[11] X. Fang, H. Peng, Small 11 (2015) 1488–1511.

[12] A. Manthiram, S.-H. Chung, C. Zu, Adv. Mater. 27 (2015) 1980–2006.

[13] A. Rosenman, E. Markevich, G. Salitra, D. Aurbach, A. Garsuch, F.F. Chesneau, Adv. Energy Mater. 5 (2015) 1500212.

[14] R. Fang, S. Zhao, Z. Sun, D.-W. Wang, H.-M. Cheng, F. Li, Adv. Mater. 29 (2017) 1606823.

[15] Z. Zeng, X. Liu, Adv. Mater. Interfaces 5 (2018) 1701274.

[16] S. Li, B. Jin, X. Zhai, H. Li, Q. Jiang, ChemistrySelect 3 (2018) 2245–2260.

[17] T. Ould Ely, D. Kamzabek, D. Chakraborty, M.F. Doherty, ACS Appl. Energy Mater. 1 (2018) 1783–1814.

[18] L. Kong, H.J. Peng, J.Q. Huang, Q. Zhang, Nano Res. 10 (2017) 4027–4054.

[19] H.-J. Peng, J.-Q. Huang, X.-B. Cheng, Q. Zhang, Adv. Energy Mater. 7 (2017) 1700260.

[20] S.-H. Chung, C.-H. Chang, A. Manthiram, Adv. Funct. Mater. 28 (2018) 1801188.

[21] S.H. Chung, A. Manthiram, J. Mater. Chem. A 1 (2013) 9590–9596.

[22] S.H. Chung, A. Manthiram, Electrochem. Commun. 38 (2014) 91–95.

[23] S.-H. Chung, A. Manthiram, Adv. Mater. 26 (2014) 1360–1365.

[24] H. Yao, G. Zheng, P.-C. Hsu, D. Kong, J.J. Cha, W. Li, Z.W. Seh, M.T. McDowell, K. Yan, Z. Liang, V.K. Narasimhan, Y. Cui, Nat. Commun. 5 (2014) 3943.

[25] C. Zu, A. Manthiram, Adv. Energy Mater. 4 (2014) 1400897.

[26] Z. Yuan, H.-J. Peng, J.-Q. Huang, X.-Y. Liu, D.-W. Wang, X.-B. Cheng, Q. Zhang, Adv. Funct. Mater. 24 (2014) 6105–6112.

[27] H.-J. Peng, W.-T. Xu, L. Zhu, D.-W. Wang, J.-Q. Huang, X.-B. Cheng, Z. Yuan, F. Wei, Q. Zhang, Adv. Funct. Mater. 26 (2016) 6351–6358.

[28] I. Raguzin, S. Choudhury, F. Simon, M. Stamm, L. Ionov, Adv. Mater. Interfaces 4 (2017) 1600811.

[29] A. Benítez, Á. Caballero, E. Rodríguez-Castellón, J. Morales, J. Hassoun, ChemistrySelect 3 (2018) 10371–10377.

[30] A. Benítez, A. Caballero, J. Morales, J. Hassoun, E. Rodríguez-Castellón, J. Canales-Vázquez, Nano Res. 12 (2019) 759–766.

[31] H. Chen, C. Wang, W. Dong, W. Lu, Z. Du, L. Chen, Nano Lett. 15 (2015) 798–802.

[32] A. Benítez, D. Di Lecce, Á. Caballero, J. Morales, E. Rodríguez-Castellón, J. Hassoun, J. Power Sources 397 (2018) 102–112.

[33] S. Waluś, C. Barchasz, J.-F. Colin, J.-F. Martin, E. Elkaïm, J.-C. Leprêtre, F. Alloin, Chem. Commun. 49 (2013) 7899.

[34] H. Kang, H. Kim, M.J. Park, Adv. Energy Mater. 8 (2018) 1802423.

[35] M.S. Garapati, A.P. V.S., R. Sundara, Carbon N. Y. 147 (2019) 364–376.

[36] A. Benítez, D. Di Lecce, G.A. Elia, Á. Caballero, J. Morales, J. Hassoun, ChemSusChem 11 (2018) 1512–1520.

[37] J.E. Knoop, S. Ahn, J. Energy Chem. 47 (2020) 86–106.

[38] Y. Ye, F. Wu, Y. Liu, T. Zhao, J. Qian, Y. Xing, W. Li, J. Huang, L. Li, Q. Huang, X. Bai, R. Chen, Adv. Mater. 29 (2017) 1700598.

[39] Y. You, W. Zeng, Y.X. Yin, J. Zhang, C.P. Yang, Y. Zhu, Y.G. Guo, J. Mater. Chem. A (2015).

[40] Q. Li, Z. Zhang, K. Zhang, J. Fang, Y. Lai, J. Li, J. Power Sources (2014).

[41] Z. Yuan, H.J. Peng, T.Z. Hou, J.Q. Huang, C.M. Chen, D.W. Wang, X.B. Cheng, F. Wei, Q. Zhang, Nano Lett. 16 (2016) 519–527.

[42] P. Zuo, J. Hua, M. He, H. Zhang, Z. Qian, Y. Ma, C. Du, X. Cheng, Y. Gao, G. Yin, J. Mater. Chem. A 5 (2017) 10936–10945.

[43] H. Lin, L. Yang, X. Jiang, G. Li, T. Zhang, Q. Yao, G.W. Zheng, J.Y. Lee, Energy Environ. Sci. 10 (2017) 1476–1486.

[44] S. Wang, J. Liao, X. Yang, J. Liang, Q. Sun, J. Liang, F. Zhao, A. Koo, F. Kong, Y. Yao, X. Gao, M. Wu, S.Z. Yang, R. Li, X. Sun, Nano Energy 57 (2019) 230–240.

[45] R.J. Wehmschulte, P.P. Power, J. Am. Chem. Soc. 119 (1997) 9566–9567.

[46] H. Yang, K. Kwon, T.M. Devine, J.W. Evans, J. Electrochem. Soc. 147 (2000) 4399.

[47] J.H. Pee, Y.J. Kim, C.Y. Kim, W.S. Cho, H.T. Kim, IOP Conf. Ser. Mater. Sci. Eng. 47 (2013) 012011.

[48] C.O. Ayieko, R.J. Musembi, A.A. Ogacho, B.O. Aduda, B.M. Muthoka, P.K. Jain, Adv. Mater. Phys. Chem. 05 (2015) 458–466.

[49] X. Li, S. Deng, M.N. Banis, K. Doyle-Davis, D. Zhang, T. Zhang, J. Yang, R. Divigalpitiya, F. Brandys, R. Li, X. Sun, ACS Appl. Mater. Interfaces 11 (2019) 32826–32832.

[50] J. Conder, R. Bouchet, S. Trabesinger, C. Marino, L. Gubler, C. Villevieille, Nat. Energy 2 (2017) 17069.

[51] J.-T. Yeon, J.-Y. Jang, J.-G. Han, J. Cho, K.T. Lee, N.-S. Choi, J. Electrochem. Soc. (2012).

[52] G. Panta, D. Subedi, Kathmandu Univ. J. Sci. Eng. Technol. 8 (2013) 31–36.

[53] T. Li, Int. J. Electrochem. Sci. (2017) 3099–3108.

[54] J. Moulder, W. Stickle, P. Sobol, K. Bomben, Surf. Interface Anal. (1981).

[55] X. Yang, J.-C. Woo, D.-S. Um, C.-I. Kim, Trans. Electr. Electron. Mater. 11 (2010) 202–205.

[56] O.A. Vargas C., Á. Caballero, J. Morales, Nanoscale 4 (2012) 2083.

[57] J. Piwowarczyk, R. Jędrzejewski, D. Moszyński, K. Kwiatkowski, A. Niemczyk, J. Baranowska, Polymers (Basel). 11 (2019) 1629.

[58] F.-Y. Zhang, S.G. Advani, A.K. Prasad, M.E. Boggs, S.P. Sullivan, T.P. Beebe, Electrochim. Acta 54 (2009) 4025–4030.

[59] D. Pantea, H. Darmstadt, S. Kaliaguine, C. Roy, Appl. Surf. Sci. 217 (2003) 181–193.

[60] T.Z. Hou, X. Chen, H.J. Peng, J.Q. Huang, B.Q. Li, Q. Zhang, B. Li, Small (2016).

[61] M. Olivares-Marín, C. Fernández-González, A. Macías-García, V. Gómez-Serrano, Energy & Fuels 21 (2007) 2942–2949.

[62] J.Q. Huang, Q. Zhang, S.M. Zhang, X.F. Liu, W. Zhu, W.Z. Qian, F. Wei, Carbon N. Y. 58 (2013) 99–106.

[63] G. Zhou, S. Pei, L. Li, D.-W. Wang, S. Wang, K. Huang, L.-C. Yin, F. Li, H.-M. Cheng, Adv. Mater. 26 (2014) 625–631.

[64] J.Q. Huang, P.Y. Zhai, H.J. Peng, W.C. Zhu, Q. Zhang, Sci. Bull. 62 (2017) 1267–1274.

Graphical abstract

This study aims to deepen the importance of the current collector used (GDL, Al foil or C-coated Al foil) when determining the performance of Li-S batteries.